IEEE Access
Multidisciplinary ⋮ Rapid Review ⋮ Open Access Journal

Received March 29, 2019, accepted April 7, 2019, date of publication April 15, 2019, date of current version April 29, 2019.

Digital Object Identifier 10.1109/ACCESS.2019.2911298

Design and Analysis of 10 MW Class HTS Exciting Double Stator Direct-Drive Wind Generator With Stationary Seal

XINKAI ZHU, (Student Member, IEEE), AND MING CHENG, (Fellow, IEEE)
School of Electrical Engineering, Southeast University, Nanjing 210096, China

Corresponding author: Ming Cheng (mcheng@seu.edu.cn)

This work was supported in part by the Postgraduate Research and Practice Innovation Program of Jiangsu Province under Project KYCX18_0092, and in part by the State Scholarship Fund of China Scholarship Council under Grant 201806090179.

ABSTRACT The superconducting (SC) generators are expected to have a promising application for offshore wind generation due to the merits of high power density and high efficiency over the conventional generators. In this paper, a 10-MW conceptual high temperature superconducting (HTS) exciting double stator direct-drive wind generator (HTS-DSDDG) with the stationary seal is proposed and investigated. The proposed HTS-DSDDG has two spatially independent stators: to place HTS field windings and copper armature windings, respectively. Thus, it realizes the stationary seal of the cooling system and removes brushes and slip rings and the other additional excitation device; hence offering the advantages of the high reliability and the low operation & maintenance cost. The main design considerations and the initial design specifications of the 10 MW HTS-DSDDG are given in detail. Furthermore, the electromagnetic characteristics of the HTS- DSDDG under no-load, rated load, and three-phase short-circuit fault conditions are analyzed by the finite element method (FEM). Subsequently, its size, weight, and cost are compared with the existing conceptual 10 MW wind generators. The results reveal that the HTS-DSDDG has excellent electromagnetic performances, such as good sinusoidal voltage, low cogging torque, and torque ripple; besides, its output power per volume is twice than that of the permanent magnet direct-drive generator (PMDDG), being comparable to that of the existing conceptual MgB_2-HTS direct-drive generators.

INDEX TERMS Double stator, stationary seal, direct-drive, high temperature superconducting (HTS), magnetic-field modulation, wind generator.

I. INTRODUCTION

The offshore wind generation is rapidly developing due to harvest wind resource in sea and increasing site restriction on load. To reduce the cost of energy, the offshore wind generators have an important trend of lighter weight and higher rating, aiming at 10 MW or beyond. The direct-drive (DD) wind turbine is expected to be enhanced substitute for the offshore wind equipment, due to the fact that the DD wind turbine uses the low-speed generator that eliminates the need of a gearbox from the turbine's drive train, offering the merits of lighter weight, higher reliability, and lower maintenance costs [1]. However, when the rating reaches to 10 MW, the size and weight of either DD electrically excited or permanent magnet synchronous generator (DD-EESG or DD-PMSG) will be very huge, hardly meeting the requirement of the large-capacity offshore wind generation.

Luckily, the use of SC windings in the DD generators permits the achievement of much stronger magnetic loading or much higher electrical loading than that in the conventional DD generators, bringing the possibility of lighter weight and smaller size [2]. The existing study indicates that the size and weight of 10 MW DD superconducting generator (DD-SCG) is roughly 50% of those of the DD-PMSG [3]. Now the DD-SCGs are regarded as one of the most viable technical approaches for large-capacity (10 MW or beyond) offshore wind turbine. The existing literature have shown some cases of DD-SCGs [4]–[14], as listed in Table 1. Nevertheless, all of the DD-SCGs in these cases are the SC synchronous generators, having a similar structure with

The associate editor coordinating the review of this manuscript and approving it for publication was Xiaodong Sun.

TABLE 1. Cases of DD-SCG.

Country	Affiliation /project	Year	Power (MW)	Speed (r/min)	SC material	Temp. (K)	Ref.
Europe	Converteam	2007	8	12	YBCO	30	[4]
Japan	Technova Inc.	2007	8	12	-	-	[5]
Japan	Niigata Univ., et al.	2011	10	10	-	-	[6]
Japan	Univ. of Tokyo	2011	10	10		-	[7]
Denmark	Technical Univ. Denmark	2011	5	12.1	-	-	[8]
USA	GE	2012	10	10	NbTi	4	[9]
Korea	Kyungook National Univ., et al.	2013	11	10	YBCO /Bi2223	-	[10]
USA	Kalsi Green Power Systems	2014	10	10	MgB2	20	[11]
China	HUST	2016	12	9	NbTi	4	[12]
Europe	SuparPower	2016	10	8.1	MgB2	20	[13]
Europe	INNWIND	2017	10	9.6	MgB2	20	[14]

the DD-EESG, and the most apparent difference between them lies that the copper field/armature windings are replaced by the SC field/armature windings. These DD-SCGs can be basically classified into two categories: the rotating SC exciting winding category and the rotating copper/SC armature winding category.

Although there has been some successful demonstrations of SC synchronous motors in the marine propulsion, a lot of critical technologies yet should be paid more cares and improved. In detail, for the category with rotating SC exciting winding, except the brushes and slip rings for DC field current connection, a coupling device for cryogenic transfer has to be installed between the rotating rotor and the stationary refrigeration system in order to realize the circulation of the coolant. The utilization of the brush-slip ring system and the rotating-seal-coupling device not only will increase the manufacture difficult and cost of generators but also will reduce the system reliability. Although both the exciting system and the cooling system can be coaxially installed with the rotor, it undoubtedly will increase the weight of the rotor system, resulting in a large rotor inertia, besides, the maintenance cost and reliability of the integrated rotor system deserve careful consideration as well. For the category with rotating copper/SC armature winding, although the rotating seal issue of the coolant can be avoided, the large armature current still has to be transferred to the rotating winding by the carbon brushes and slip rings. Actually the design and fabrication of the large-current-brush-slip ring system is a very hard work, in addition, it is no doubt that as long as the brush-slip ring system exists, and the SC generators must have a relative higher O&M cost and a lower system reliability.

In order to solve the aforementioned critical and tricky issues existed in the SC generators, a kind of SC generator/motor based on the magnetic-field modulation principle have attracted more and more attention. In [15], a HTS flux-switching machine (HTS-FSM) for wind energy conversion was proposed by introducing HTS windings to replace the PMs in the FSPM machines, realizing the brushless and stationary-seal at the same time. In [16],

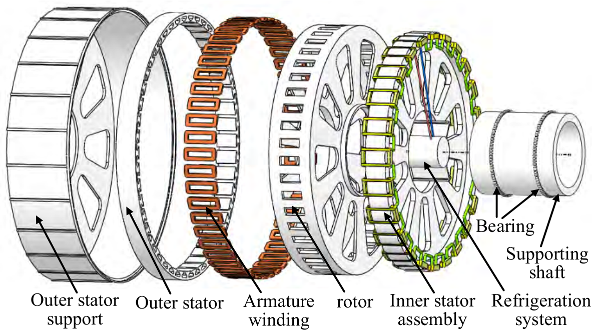

FIGURE 1. 3-D exploded model of the 10 MW HTS-DSDDG.

a segmented-rotor HTS flux-switching generator (HTS-FSG) was designed, fabricated, and tested. It shows the feasibility of the technical route of HTS-FSG. Then different topologies of the HTS-FSG were proposed and analyzed, in [17], [18]. In order to make fully use of internal vacancy to further improve the power/torque density, the dual-rotor or dual-stator HTS-FSMs were also successively investigated in [19], [20]. Since the volume of cryostat used in SC machine is relative large, in order to deal with the space limitation, a HTS claw-pole vernier machine with one annular SC coil was proposed and analyzed in [21]. This kind of modulation HTS machines have also attracted lots of attention in the wave energy generation, a linear doubly-salient HTS machine was proposed and investigated in detail in [22]. Then the different topologies of the linear modulation machine were continuously proposed and analyzed in [23]–[26].

Although lots of works have been done about the modulation HTS generator/motor, almost all of them focus on analysis of the small-scale small-rating machines. Up to now, the large-rating modulation HTS wind generators, like 10 MW, have not been reported and investigated. Therefore, the purpose of this paper is to study the feasibility of a 10 MW HTS double-stator direct-drive wind generator (HTS-DSDDG). In section II, the main design considerations of the 10 MW HTS-DSDDG will be discussed. In section III, the design specifications and electromagnetic characteristics of the 10 MW HTS-DSDDG will be given and analyzed in detail by finite element method (FEM). Then in section IV, the size, weight and cost of the HTS-DSDDG will be analyzed, and compared with the existing conceptual 10 MW wind generators. Finally, some conclusions will be drawn in section V.

II. DESIGN CONSIDERATIONS OF THE PROPOSED HTS GENERATOR

A. TOPOLOGY AND ASSEMBLY

The 3-D exploded model of the 10 MW HTS-DSDDG is shown in Fig. 1. It can be seen that the two ends of the rotor are connected with the supporting shaft by two bearings. The inner stator assembly is amounted in the cavity of the rotor, including the inner stator support structure, core, HTS field windings, and the cooling system. Then the cup-shaped outer stator support holding the outer stator iron with the copper armature winding is located at the left end of the supporting shaft. It should be noted that the polarity of all HTS field windings is the same, i.e., N poles or S poles. It is worth noting that although the rotor is sandwiched between two stators, it is possible to realize the two-end-connection of rotor and shaft to keep the mechanical strength to withstand the wind gusts, for example, the proposed conceptual design as shown in Fig. 1. Of course, some mechanical issues still need to be carefully considered by mechanical designer.

Additionally, it can be seen that all cryogenic Dewars (indicated in yellow) containing HTS field windings are placed on the inner stator, and connected by the cryogenic tube (indicated in green), and cooled by the coolant from the refrigeration system via the cryogenic tube, where the red and blue tubes realize the circulation of the coolant. Both the refrigeration system mounted in the cavity of the supporting shaft and the Dewars are stationary, hence realizing the stationary seal of the cooling system and the brushless of the exciting system at the same time due to the double-stator structure, which may greatly improve the reliability and reduce the cost of the generator system.

B. SUPERCONDUCTING WIRES

The low temperature superconductor (LTS), such as NbTi and Nb_3Sn, have been widely applied in the magnetic resonance imaging (MRI) and various high-field magnet systems. However, these LTSs require very low operating temperatures, in the range of 1.8-4.2 K, the efficiency of the cooling system working at such temperatures is very low, resulting in the high cost and the low reliability, so limiting their widespread application. Compared with the LTSs, the high temperature superconductor (HTS), such as Bi2223, YBCO and MgB_2, are much more promising options. However, YBCO wire is prone to be damaged due to its coated structure, and currently its price is relatively high. Compared with YBCO wire and Bi2223 wire, the MgB_2 wire has the merits of low cost, but its critical current is small under the high applied magnetic field, besides it is not available in China at present. Therefore, after carefully thinking over all commercial superconducting wires, the filed winding of the HTS-DSDDG will employ the Bi2223 wire, whose main parameters and properties with applied magnetic field have been descripted in detail in [16].

C. POLE-PAIR COMBINATION

The operation principle of the HTS-DSDDG is consistence with the airgap field modulation theory [27]. Like vernier machine, partitioned-stator machine, and flux-switching machine, the pole-pair combination of the HTS-DSDDG must satisfy the relationship of $p_s + p_f = p_r$, where p_s is the pole-pair number of the armature winding, p_f is the pole-pair number of the SC field winding, and the p_r is the pole-piece number of the rotor.

The pole-pair combination of the partitioned-stator machine, vernier machine and flux-switching machine have been investigated, showing that this pole-pair combination of 12-stator-slot with 11-rotor-pole-piece, namely, the stator has 12 slots and the rotor evenly has 11 magnetic blocks and 11 non-magnetic blocks in the circumferential direction, can output the maximum torque with minimum torque ripple [28]. Although the 11-rotor-pole option will suffer from unbalanced magnetic force (UMF), it can be relieved by multiplying both the stator slot and rotor pole-piece numbers to achieve an even rotor pole-piece number.

To satisfy the above mentions, modular structure will be employed in the HTS-DSDDG, which consists of even number of modules. The pole-pair combination of each module is 12-stator-slot with 11-rotor-pole-piece. However, the pole-pair number of the HTS-DSDDG could not be set as a very big number, due to the big size of HTS coils and Dewar, caused by the critical bending radius of the SC wire. Otherwise, the diameter of the HTS-DSDDG will be very large. The existing literature indicates that the diameter of a SCDDG with 48 separated modular Dewars is about 10 m [2]. To meet the design requirement, namely, even number of modules and the diameter of generator below 10 m, the pole-pair combination of the HTS-DSDDG will be set as 48-stator-slot with 44-rotor-pole-piece, in which the number of module is 4 and the number of modular Dewar is 24.

D. MAGNETIC/ELECTRICAL LOADING

The electromagnetic torque T_e can be expressed as

$$T_e = \frac{\pi}{2} D^2 L \sigma \rightarrow \sigma \propto B \cdot A \tag{1}$$

it is proportional to the average shear stress σ, the air gap diameter D and the active length L of a machine, where the average shear stress σ is proportional to the magnetic loading B (average air gap magnetic flux density) and the electrical loading A (linear current density) of a machine. To limit the size of the generator (D or L), the σ needs to be increased by increasing either the B or A.

The HTS-DSDDG employs the Bi2223 field windings to generate the stronger B. However, the definition of the B of the HTS-DSDDG is different from the conventional SC generators, since the operation principle of the HTS-DSDDG is based on the airgap field modulation theory. The B of the HTS-DSDDG will be given in detail in part A of section III.

The design of the A of the HTS-DSDDG has a close relationship with the cooling method employed by the armature windings. Usually, the forced-air cooling method is adopted for the armature winding of large wind generator, which limits the electrical loading below $A = 75$kA/m and the current density of armature winding below $J = 3$ A/mm^2. The heat loading can be calculated by

$$\text{Heat loading} = A \cdot J \tag{2}$$

Therefore, if the forced-air cooling method is employed, the heat loading of the HTS-DSDDG should not exceed the $22.55 \times 10^{10} \mathrm{A}^2\mathrm{m}^3$.

The A is defined as the number of conductor-current per unit circumferential length of airgap, it can be expressed as

$$A = \frac{mNI_{rms}}{\pi D_{air}} \tag{3}$$

where m is the phase number of machine, N is the number of series turns per phase, I_{rms} is the rms value of armature current, D_{air} is the diameter of airgap.

The J is denoted as the current per square meter of copper wire used in armature winding, it is obtained as

$$J = \frac{I_{rms}}{S_{slot} \cdot S_{fill}} \tag{4}$$

where S_{slot} and S_{fill} are the section area and the filling factor per stator slot, respectively.

Hence, the heat loading can be reformed as

$$A \cdot J = \frac{mNI_{rms}}{\pi D_{air}} \cdot \frac{I_{rms}}{S_{slot} \cdot S_{fill}} \tag{5}$$

Additionally, the power rating of generator with power factor of 1 can be expressed as

$$P_e = \mathrm{m} \cdot U_{rms} \cdot I_{rms} = \frac{m}{\sqrt{2}} \cdot 4.44 \frac{\Omega_r P}{60} N \emptyset K_w \cdot I_{rms} \tag{6}$$

where U_{rms} is the rms value of phase voltage of armature winding, f is the frequency of phase voltage, Ω_r is the rotating speed of machine, P is the pole-pair number of machine, $\emptyset$ is the flux per phase winding, K_w is the winding factor of armature winding.

For a specific wind generator, its voltage level and the rotating speed have been determined, on the other words, both the voltage U_{rms} and the rotating speed Ω_r are industrial standard values. Therefore, the variation range of the N and the I_{rms} is very limited after the magnetic loading is determined. Hence, in the identical thermal condition, in order to adjust the combination of A and J, the D_{air} and the S_{slot} are two main regulated parameters, as indicated in formula (5).

Since the proposed DSDDG adopts the double-stator structure, the diameter of the outer airgap adjacent to the armature winding can be set as relatively small. It means that the S_{slot} would become bigger to allow the same turn number of armature coils with a bigger cross-section area of copper wire, due to the smaller diameter of outer airgap.

However, it should be noted that the higher A could reduce the size of the HTS-DSDDG according to (1) and lower current density J could keep higher efficiency due to lower Joule losses of the armature winding, but this means larger slot area of stator and more copper wires have to be needed. After carefully weighting the size of the HTS-DSDDG and the amount of copper wires, the electrical loading A and the current density J of the HTS-DDDSG are decided to be 113 kA/m and 1.77 A/mm2, respectively.

E. CRYOGENIC DEWAR

There are two kinds of conceptual design of cryogenic Dewar: one is that all the SC coils are set in a single vacuum vessel, called as integrated Dewar [9]; the other one is that each SC coil has an independent vacuum vessel, called as modular Dewar [29]. Nevertheless, when transforming the conceptual design to reality, the integrated Dewar will lead to other practical problems to challenge the transportation, installation, maintenance, especially for the large-scale SCDDGs with a large diameter, hence the modular concept attracts more attention in the SCDDGs. In the HTS-DSDDG, a modular Dewar will be also developed, the section drawing of the Dewar is shown in Fig. 2, which is mainly referred to the design in [29]. In detail, the outer box thickness is assumed 10 mm to satisfy the mechanical requirement. The inner box thickness is assumed 20 mm to accommodate cooling channels. The multi-layer insulation (MLI) & vacuum of thickness of 20 mm is accommodated between the outer and inner boxes made of stainless steel.

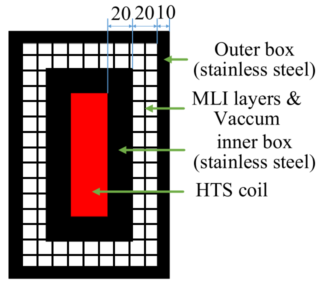

FIGURE 2. The cross section of the modular Dewar used in the HTS-DSDDG.

III. ELECTROMAGNETIC PERFORMANCE OF THE PROPSOED HTS GENERATOR

Connected with the wind turbine with a diameter of 178 m, the rotor speed of generator is limited to be 9.6 r/min for a safe tip speed of wind turbine blade [30]. Besides, there are lots of losses in the generator, such as armature winding DC and AC loss, iron loss, refrigeration power, cooling air blower's power and so on, so its efficiency is estimated to be 95% [3]. Based on the aforementioned design considerations and proper design process [31], the initial design specifications of the proposed HTS-DSDDG are obtained as listed in Table 2. And the geometry of the HTS-DSDDG is shown in Fig. 3.

Electromagnetic performance of the HTS-DSDDG at no load, rated load, and three-phase short-circuit fault conditions have been studied by the FEM. Due to the symmetry of the generator, the simulation model has been reduced to 1/4 of the generator.

A. NO-LOAD PERFORMANCE

The outer airgap flux density waveform at the rated field current is shown in Fig. 4. It can be found that the maximum flux density is about 2.2 T. However, according to the airgap field modulation theory [27], the average value of airgap flux density can't be used as the magnetic loading. The corresponding flux density spectrum without 51st or beyond is shown in Fig. 5. It can be seen that the outer airgap flux

TABLE 2. Specifications and initial design parameters of the HTS-DSDDG.

Symbol	Parameters	Value	Unit
P_N	Rated power	10	MW
n_N	Rated rotating speed	9.6	r/min
T_N	Rated torque	11	MN·m
V_N	Line voltage of armature winding	4000	Vrms
I_N	Phase current of armature winding	2545	Arms
J	Current density of armature winding	1.77	A/mm^2
R	Phase resistance of armature winding	0.02	Ω
As	Slot filling factor of outer stator	0.6	-
A	Electrical loading	113	kA/m
B	Magnetic loading	1.99	T
f	Rated frequency	7	Hz
η	Rated efficiency	95%	-
cos(φ)	Power factor	1	-
	Armature winding configuration	3-phase	-
	Armature winding cooling method	Forced air cooling	-
D_{osod}	Outer diameter of outer stator	10.26	m
D_{osid}	Inner diameter of outer stator	9.6	m
h_r	Radial thickness of sandwiched rotor	150	mm
h_{mrr}	Radial thickness of magnetic ring	80	mm
h_{mrth}	Tip height of magnetic ring	25	mm
h_{ist}	Height of inner stator teeth	120	mm
b_{ist}	Width of inner stator teeth	470	mm
h_{isy}	Radial thickness of inner stator yoke	150	mm
h_{sc}	Height of HTS field winding	100	mm
b_{sc}	Width of HTS field winding	30	mm
g_o	Length of outer airgap	10	mm
g_i	Length of inner airgap	10	mm
l	Active axial length	800	mm
N_{oss}	Slot number of outer stator	48	-
N_{iss}	Slot number of inner stator	48	-
P_{arm}	Pole-pair number of armature winding	20	-
P_r	Pole-piece number of rotor	44	
N_D	Number of Dewar	24	
	Polarity of HTS field coils	Same polarity	-
$F_{HTS\text{-}coil}$	MMF per HTS magnetic pole	250000	AT
	Superconducting materials	Bi2223	-
T_{oper}	Operation temperature of HTS coil	30	K

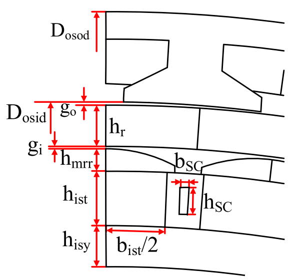

FIGURE 3. Geometry of the HTS-DSDDG.

density contains a number of stationary and rotating harmonic components, due to the modulation of sandwiched rotor, inner and outer stator teeth. Due to the magnetic gearing effect in the DSDDG [32], the armature reaction also will generate a lot of stationary and rotating harmonic components after the modulation of sandwiched rotor, inner and outer stator teeth. As it known, the armature reaction harmonics and the excitation harmonics, which have the same order, the same rotating speed and direction, can interact each other to output constant electromagnetic torque. Throughout the harmonic analysis, it is found that only these harmonics, 5th, 6th, 7th, 18th, 299th, and 41st, indicated by red fonts in Fig. 5, can contribute to the constant electromagnetic torque.

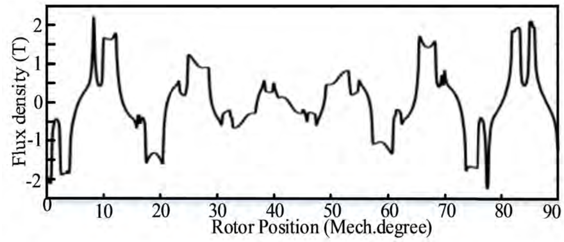

FIGURE 4. The radial flux density distribution in the middle of the outer airgap with the rated field current.

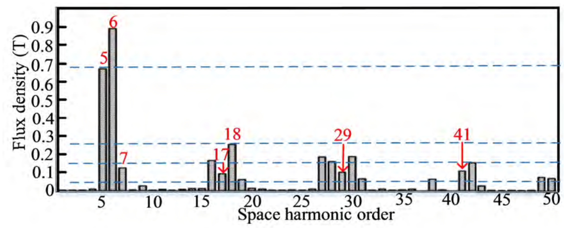

FIGURE 5. The radial flux density spectrum in the middle of the outer airgap with the rated field current.

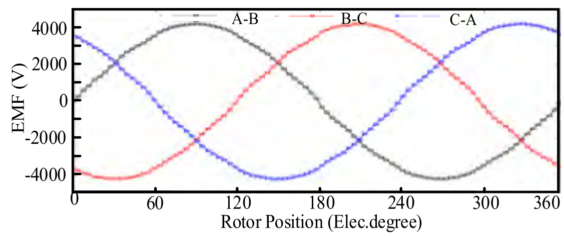

FIGURE 6. The EMF waveform with the rated field current.

Therefore, these harmonics, 5th, 6th, 7th, 18th, 29th, and 41st, usually are regarded as the effective harmonics, whose magnitude are 0.672 T, 0.89 T, −0.124 T, 0.092 T, 0.253 T, 0.101 T, 0.107 T, respectively, in which the negative sign denotes the opposite rotating direction, meaning that the 7th harmonic will generate an opposite electromagnetic torque with the other order harmonics. The sum of their magnitude can be regarded as the magnetic loading, 1.99 T. The corresponding EMF at the rated field current is shown in Fig. 6. Although there are a number of harmonics in the outer airgap flux density, the EMF waveform is very sinusoidal. The THD of the EMF is about 1.7%, which is very small.

The cogging torque is a crucial index for wind power generator, since it will determine the cut-in speed of the wind turbine. The cogging torque cycles n_m per mechanical period is the least common multiple (LCM) of stator slot number (N_s) and rotor piece number (N_r)

$$n_m = \mathrm{LCM}(N_s, N_r) \tag{7}$$

Consequently, the cogging torque cycles n_e per electric period can be obtained by [27].

$$n_e = \frac{\mathrm{LCM}(N_S, N_r)}{N_r} \tag{8}$$

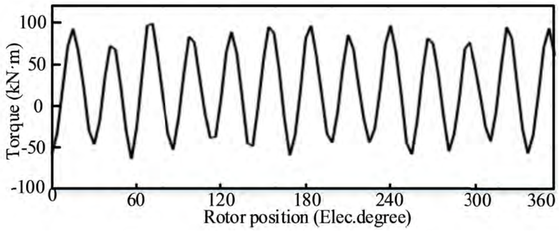

FIGURE 7. The cogging torque waveform with the rated field current.

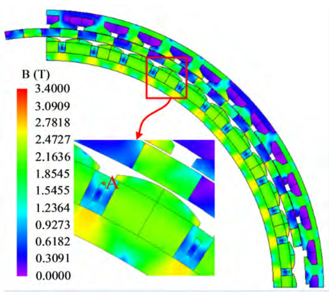

FIGURE 8. The magnetic field map of 1/4 model of the HTS-DSDDG under the rated load condition.

The simulated cogging torque at the rated field current in one electric period is given in Fig. 7, the cogging torque cycles is 12, being consistence with the previous analysis. And the peak-peak value of cogging torque is about 150 kN·m, only 1.36% of the rated torque.

B. RATED LOAD PERFORMANCE

The magnetic field map corresponding to 1/4 model of the HTS-DSDDG under the rated load condition is presented in Fig. 8. It can be seen that the inner stator yoke is the most saturated part with a maximum value of 2.7 T (not taking into account the tips of magnetic ring and rotor-iron-piece), the average magnetic field density of iron pole is about 2.2 T, and the peak magnetic field in the region A of superconducting coils, marked by the red circle, is 1.85 T. Although the magnetic field density of inner stator yoke is very high, and there is a rich harmonic content in the airgap, frequencies of harmonics with higher magnitude are relatively very low due to the low rotating speed of 9.6 r/min and the low pole-pair number of 44. The iron loss is proportional to the frequency [33]–[35], so the iron loss is relatively low due to the lower frequency. It should be note that the operation point (I, B, T) of the SC coils is one of the most important parameters for a SCG, and these parameters are always interdependent. It is a fact that there are lots of harmonics near the SC coils, as shown in Fig. 5, and they will induce AC loss in the SC coils, further affecting the determination of operating temperature T and the operating current I. Of course, the design and installation of the SC coils in the Dewar are also critical discussion points. But the analysis of AC loss and the design of SC coil are not the key objects of this paper, these works will be investigated in detail in next papers. In this paper, the method of comparing the load line of the SC coil and the J-B⊥ characteristic of Bi2223 wire at different cooling temperatures is adopted to find the final operation point (I, B, T) of the SC coil. After carefully thinking over the comparisons, it is found that the cooling temperature of 30 K can meet the requirement of electromagnetic performance, and keep the higher carrying current capacity of the SC coil at the same time. Therefore, considering the load line of HTS coil and the J-B ⊥ characteristic of Bi2223 wire at 30 K with 30 % safety margin, as shown in Fig. 9, the coil operation point, namely the cross point of red line and blue line, has been established at 100 A and 1.9 T.

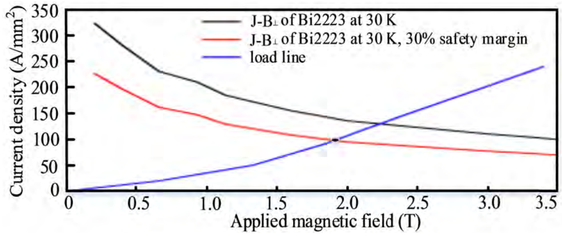

FIGURE 9. The operation point of the HTS coil of the HTS-DSDDG.

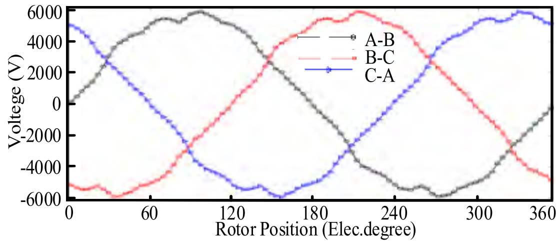

FIGURE 10. Voltage waveform under the rated load condition.

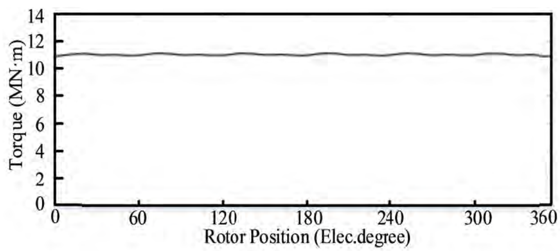

FIGURE 11. Torque waveform under the rated load condition.

For a generator, the output voltage waveform is one of the important performance indicators. The voltage waveform under the rated load condition are shown in Fig. 10, the THD of voltage is about 4.6%, which basically can satisfy the generation requirement. Moreover, the torque waveform at the rated load is shown in Fig. 11. The average torque is about 11 MN · m, meeting the design requirement of generator.

C. SHORT-CIRCUIT FAULT PERFORMANCE

Among the usually-confronted faults, three-phase short-circuit is the most stressful. The analysis of performances under fault operation is conducted in the condition of the Bi2223 field winding excited by current source.

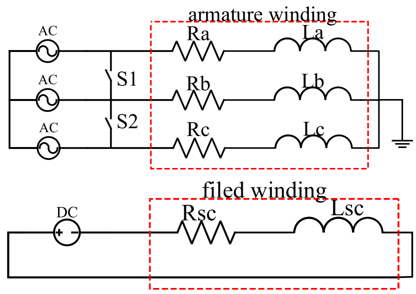

FIGURE 12. Connection diagram of the HTS-DSDDG with current exciting source.

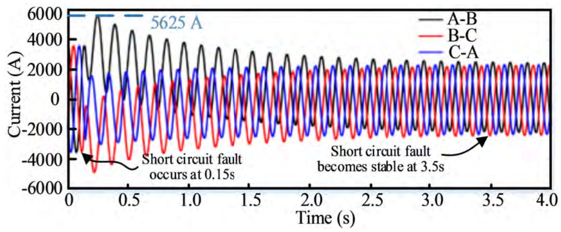

FIGURE 13. The armature current waveform under the three-phase short-circuit fault condition.

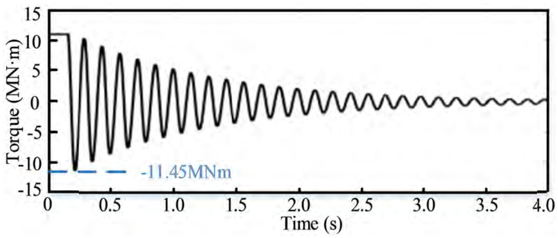

FIGURE 14. The torque waveform under the three-phase short-circuit fault condition.

The connection diagram is shown in Fig. 12. Before the short-circuit fault arises, the HTS-DSDDG operates at the rated status, with rated three-phase currents imposed into the armature winding. At 0.15 s, the switch (S1 and S2) are closed to simulate the three-phase short-circuit fault. Due to the rotor inertia, the rotor speed will keep constant, 9.6 rpm, at the moment of short circuit.

The responses of torque and stator current at three-phase short-circuit fault are shown in Fig. 13 and Fig. 14, respectively. The peak value of the torque and the armature current are 11.45 MN · m and 5625 A, respectively. The peak armature current under the short-circuit fault condition is increased to 1.56 times of that of the rated value, and the peak value of the short-circuit torque is increased from 11.1 MN · m (the rated status) to 11.45 MN · m, so the increase of the torque is very small.

IV. SIZE, WEIGHT, AND COST OF THE PROPOSED HTS GENERATOR

A. SIZE, WEIGHT, AND COST

The size of the HTS-DSDDG is referring to the diameter and active length of the generator. The weight of the

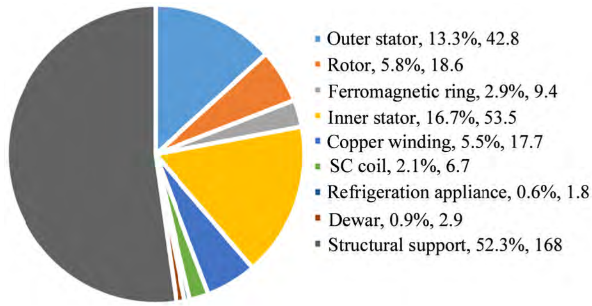

FIGURE 15. Mass of the HTS-DSDDG components, unit (ton).

TABLE 3. The unit cost of materials used in the HTS-DSDDG.

Material	Unit cost[a]
Copper	11.6 $/kg
Silicon steel	1.6 $/kg
Structural steel	1.2 $/kg
Bi2223 wire	22 $/m
MgB_2 wire	3.5 $/m
PM (NdFeB)	28.9 $/kg

[a] The price of the MgB_2 wire refers to the information received from the Columbus Superconductors SpA, and the prices of the other materials refer to the current market price in China.

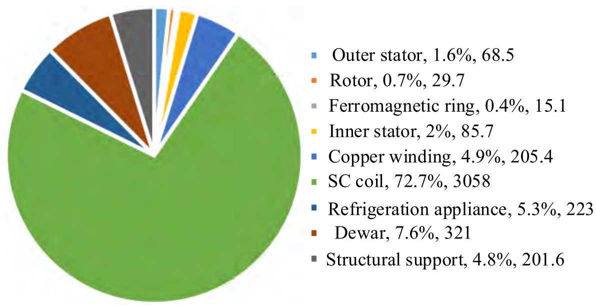

FIGURE 16. Cost of the HTS-DSDDG components, unit (k$).

HTS-DSDDG is referring to the sum of the active and structural materials mass, where the active materials mass consists of iron, copper, Dewar, coolant and cryogenic refrigeration system mass, while the structural materials consists of stator arm, rotor arm, stator cylinder and rotor cylinder [36]. Besides, the cost of the HTS-DSDDG is determined by the active and structural mass and assumed unit costs of materials.

Since there has not been commercial demonstration of 10 MW class superconducting wind generator, it is difficult to accurately estimate the mass and cost of structural support, Dewar and refrigeration system of the HTS-DSDDG, so their estimation will refer to the mass and cost estimation of those of 10 MW MgB_2 SCDDG descripted in [36]. The mass of the HTS-DSDDG components is shown in Fig. 15. It can be seen that the total mass of the HTS-DSDDG is 321.47 tons, of which the percentage of structure support mass is the maximum, up to 52.3%, 168 tons. Then the mass of silicon steel is the second biggest percentage, it reaches 38.7%, including outer stator 13.3%, rotor 5.8%, ferromagnetic ring 2.9% and

TABLE 4. Comparison of the HTS-DSDDG with the existing 10 MW class conceptual wind generators [2], [12], [36].

Generator type	The proposed HTS-DSDDG	LTS-SCDDG	MgB_2-SCDDG	MgB_2-SCDDG	YBCO-SCDDG	PPMDDG	PMDDG
Project	NSFC	NSFC	Suprapower	INNWIND	INNWIND	INNWIND	INNWIND
Power (MW)	10	12	10	10	10	10	10
Speed (r/min)	9.6	9	8.1	9.6	9.6	9.65	9.6
Outer diameter (m)	10.26	7.34	10.1	8.4	7	6	10
Axial length (m)	0.8	1.02	0.744	1.3	1.2	1.7	1.68
Output power per volume (kW/m^3)[a]	151	278	168	139	217	208	76
Output power per mass (kW/ton)	31	96	23	35	-	67	42
Superconducting (SC) wire	Bi2223	NbTi	MgB_2	MgB_2	YBCO	-	-
Length of SC wire (Km)	139	-	153.6	21.25	5.35	-	-
Permanent magnet (NdFeB)	-	-	-	-	-	yes	yes
Dewar structure	modular	integrated	modular	modular	modular	-	-
Dewar seal method	stationary	stationary	rotating	rotating	rotating	-	-
Rotating armature winding	-	yes	-	-	-	-	-
Rotating field winding	-	-	yes	yes	yes	-	-
Brush and slip ring	-	yes	yes[b]	yes[b]	yes[b]	-	-
Torque tube	-	yes	-	-	-	-	-
Stator core material	iron	air	air	iron	iron	iron	iron
Rotor core material	iron	iron	iron	iron	iron	iron	iron
Generator mass (ton)							
Copper winding mass	17.7	19.2	22.81	13.1	-	7	13.64
Silicon steel mass	124.3	48	84.53	101.2	-	29.5	48.93
Superconducting wire mass	6.7	9.2	7.37 [37]	0.32	-	-	-
NdFeB mass	-	-	-	-	-	13.5	6.4
Coldheader &compressor mass	1.8[c]	4	1.8[c]	1.8	-	-	-
Cryostat mass	2.9	45.2	11.18	3.4	-	-	-
Active structure mass	153.4	125.6	127.7	119.8	156	50	68.97
Support structure mass	168[c]	64.1	282.5	168	-	100	168
Total mass	321.4	189.7	410.2	287.8	-	150	236.97
Generator cost estimation (thousand dollars) [d]							
Copper winding cost	205.32	222.72	264.6	151.96	-	81.2	158.22
Silicon steel cost	198.88	76.8	135.25	161.92	-	47.2	78.29
Superconducting wire cost	3058	290.3 [12]	537.6	74.38	618.46 [36]	-	
NdFeB cost	-	-	-	-	-	390.15	184.96
Coldheader & compressor mass	223	632.3	-	223	-	-	-
Dewar cost	321	656.2	-	377	-	-	-
Support structure cost	201.6	76.92	339	201.6	-	120	201.6
Total cost	4207.8 (1636.3[e])	1955.24	1276.44[f]	1189.86	-	518.55	421.47

[a] The volume is equal to the $3.14 * D^2 * L/4$, where D indicates the diameter and L indicates the axial length.
[b] Depend on the exciting system, brush and slip, rotating transformer or the other devices.
[c] Refer to the mass of the coldheader & compressor and support structure of the MgB_2-SCDDG in the INNWIND project.
[d] The unit cost of copper, silicon steel, superconducting wire, NdFeB, and support steel is referring to the unit cost of materials like that listed in Table III, except for the cost of the superconducting wire of the LTS-SDCCG and the YBCO-SCDDG.
[e] The total cost of the proposed HTS-DSDDG when using MgB_2 wire.
[f] The total cost of the MgB_2-SCDDG of the Suprapower project don't include the cost of the coldheader & compressor and the Dewar.

inner stator 16.7%, so it can be seen that the percentage of silicon steel usage of outer and inner stator is bigger. Therefore, if air-core outer or inner stator is adopted in the HTS-DSDDG, its total mass would be considerably reduced. However, the amount of SC wire will be increased by several times to produce the same air gap magnetic flux density as that in iron-core stator one, due to the high magnetic reluctance of air. After comparison analysis, it has been found that if the air-core inner stator is employed, the total mass of the HTS-DSDDG will approximately reduce 10%, but the amount of SC coils will be about 5 times of the initial amount.

We assume the unit cost of materials used in the HTS-DSDDG like that listed in Table 3. Consequently, the cost of the HTS-DSDDG components is given in Fig. 16. It can be seen that the total cost of the HTS-DSDDG is 4208 k\$, of which the cost of SC coil has a biggest percentage, up to 72.7%, 3058 k\$. Next the cost percentage of Dewar and refrigeration appliance is 7.6% and 5.3%, respectively. Since the structural support depends on the aerodynamic performance of wind turbine, its cost reduction is very limited [30]. Nevertheless, if low-cost HTS wire, such as MgB_2, is employed in the HTS-DSDDG, or the critical current of Bi2223 could be improved several times, the total cost of the HTS-DSDDG would be sharply reduced. For example, if MgB_2 wire at the price of 3.5 dollars per meter in Table 3 could be employed, the cost of SC coil will be reduced by 84.1%, or 2571.5 k\$, consequently, the total cost of the HTS-DSDDG will be 1636.5 k\$. But at present, the MgB_2 wire is not available in China. If the MgB_2in the future is widely used, it will greatly promote the development of HTS generator.

B. COMPARISON WITH EXISTING CONCEPTUAL DESIGNS

In order to sufficiently illustrate the feasibility and application potential of the proposed HTS-DSDDG, it will be compared with several existing 10 MW conceptual designs, as shown in Table 4. The PMDDG is the option I of reference PMDDG of INNWIND project [36], and the PPMDDG is the pseudo permanent magnet DD generator.

It can be seen from Table 4 that the manufacturing cost of the SCDDGs and the PPMDDG are all higher than that of the PMDDG, since the expensive superconducting wire or more permanent magnet are needed in the SCDDGs or the PPMDDG. However, the manufacturing cost of the generator is only a small proportion of the total cost of wind power generation system, whose total cost includes the equipment cost, infrastructure cost, operation & maintenance cost. Therefore, from a perspective of reducing the total cost of wind power generation system, if the wind generator offers the merits lighter weight (higher output power per mass), smaller volume (higher output power per volume), higher reliability (brushless and stationary seal), and easier maintenance, the total cost may be reduced, even if the original manufacturing cost of the generator is high.

As far as the output power per volume is concerned, the output power per volume of the SCDDGs and the PPMDDG are all higher than that of the PMDDG. The output power per volume of the proposed HTS-DSDDG is much twice of that of the PMDDG, almost being comparable to the MgB_2-SCDDGs designed by the Suprapower and the INNWIND. In terms of output power per mass, the proposed HTS-DSDDG is about 26% lower than that of the PMDDG, being equivalent to the MgB_2-SCDDG of INNWIND and about 34.8% higher than that of the MgB_2-SCDDG of Suprapower, due to the fact of the lower speed of the MgB_2-SCDDG of Suprapower, only 8.1 r/min. In addition, although the output power per volume and the output power per mass of the proposed HTS-DSDDG are both lower than the LTS-SCDDG, the LTS-SCDDG needs extremely low operating temperature, resulting in the more complex cooling system and higher maintenance cost. The existing study indicates that the manufacturing cost of LTS generator is 2 million dollars, but the operation and maintenance cost for 25 years is 1.6 million dollars [12].

Therefore, from a perspective of the whole lifetime cost of wind turbine, the proposed HTS-DSDDG and the other HTS-SCDDGs may be more prospect than the LTS-SCDDG. In addition, it should be noted that the PPMDDG also exhibits great improvement in the output power per volume or per mass, which will be also a promising approach for wind generator.

It is worth noting that the output power per volume or per mass of the proposed HTS-DSDDG approximately matches to those of the MgB_2-SCDDG designed by INNWIND, however, the HTS-DSDDG realizes the stationary seal of the Dewar, bringing the prospect of reducing the manufacturing difficulty and cost, and improving reliability of the cooling system. Moreover, it also eliminates brushes and slip rings or the other additional excitation equipment. Taking into account the reliability and maintainability of the cooling system and the brush-slip ring system, the proposed HTS-DSDDG will exhibit obvious advantages and is expected to reduce the operation and maintenance costs of the SCDDGs. Besides, it is worthy to point out the volume of the HTS-DSDDG can be reduced by about 50%, compared with the 10MW PMDDG, so it probably may play an important role in space-constrained applications, such as ship propulsion in addition to wind turbine.

V. CONCLUSION

This paper studies the feasibility of 10 MW HTS-DSDDG for wind power generation. The main design considerations and the initial design specifications of the HTS-DSDDG are given, and analyzed by FEM, then compared with the existing conceptual 10 MW wind generators. Some research results may be highlighted as follows:

(1) Since the specific design parameters of the existing designs/models are incomplete, the comparison of electromagnetic performance had not been conducted, but it can be affirmed that the proposed HTS-DSDDG has good electromagnetic performance, such as, good sinusoidal voltage, low cogging torque and torque ripple, low short-circuit current and torque, which basically meet the requirement of wind generator.

(2) At present, the cost of the proposed HTS-DSDDG is much higher than that of the PMDDG, mainly due to the expensive HTS wire. Although HTS materials are expensive and difficult to manufacture, the use of them can reduce the size and weight of wind generator, and correspondingly reduce the requirements and costs of wind turbine tower, infrastructure, etc., as well as transportation and installation costs, probably leading to the cost reduction of the entire generation unit.

(3) The output power per volume of the proposed HTS-DSDDG is about twice as much as that of the PMDDG, but its output power per mass is slightly lower than that of the PMDDG. It should be noted that if the air-core inner stator is adopted, its output power per mass will be increased, but at the cost of more superconducting wires.

(4) The power density per volume/mass of the HTS-DSDDG is lower than that of the LTS-SCDDG designed by HUST, but its operation & maintenance cost will be much lower than that of the LTS-SCDDG. Hence, from a perspective of the whole lifetime cost of the wind turbine, the HTS-DSDDG will be a more promising approach.

(5) The power density of the HTS-DSDDG is comparable to that of the MgB_2-SCDDGs designed in

the Suprapower project and the INNWIND project. However, it is worth noting that the HTS-DSDDG realizes the stationary seal of the cooling system and eliminates the brush-slip ring system, which will greatly reduce the manufacturing difficulty and operation & maintenance cost of the generator system.

Therefore, according to the above research results, it is worthy to point out that the proposed HTS-DSDDG will be a very promising solution for offshore wind generation, while further studies will be needed before it can be applied in the industry, for example, calculation of AC loss, analysis of mechanical strength, and design of SC coil.

REFERENCES

[1] M. Cheng and Y. Zhu, "The state of the art of wind energy conversion systems and technologies: A review," *Energy Convers. Manage.*, vol. 88, pp. 332–347, Dec. 2014.

[2] I. Marino *et al.*, "Lightweight MgB_2 superconducting 10 MW wind generator," *Supercond. Sci. Technol.*, vol. 29, no. 2, Dec. 2015, Art. no. 024005.

[3] R. Fair *et al.*, "Superconductivity for large scale wind turbines," GE Global Res., Niskayuna, NY, USA, Tech. Rep. DOE-EE0005143, Apr. 2012.

[4] C. Lewis and J. Müller, "A direct drive wind turbine HTS generator," in *Proc. IEEE Power Eng. Soc. Gen. Meeting*, Jun. 2007, pp. 1–8.

[5] N. Maki, "Design study of high-temperature superconducting generators for wind power systems," *J. Phys., Conf. Ser.*, vol. 97, no. 1, 2008, Art. no. 012155.

[6] S. Fukui *et al.*, "Study of 10 MW-class wind turbine synchronous generators with HTS field windings," *IEEE Trans. Appl. Supercond.*, vol. 21, no. 3, pp. 1151–1154, Jun. 2011.

[7] Y. Terao, M. Sekino, and H. Ohsaki, "Electromagnetic design of 10 MW class fully superconducting wind turbine generators," *EEE Trans. Appl. Supercond.*, vol. 22, no. 3, Jun. 2012, Art. no. 5201904.

[8] A. Abrahamsen *et al.*, "Feasibility study of 5 MW superconducting wind turbine generator," *Phys. C, Supercond. Appl.*, vol. 471, nos. 21–22, pp. 1464–1469, Nov. 2011.

[9] W. Stautner *et al.*, "Large scale superconducting wind turbine cooling," *IEEE Trans. Appl. Supercond.*, vol. 23, no. 3, Jun. 2013, Art. no. 5200804.

[10] H.-J. Sung *et al.*, "Practical design of a 10 MW superconducting wind power generator considering weight issue," *IEEE Trans. Appl. Supercond.*, vol. 23, no. 3, Jun. 2013, Art. no. 5201805.

[11] S. S. Kalsi, "Superconducting wind turbine generator employing MgB_2 windings both on rotor and stator," *IEEE Trans. Appl. Supercond.*, vol. 24, no. 1, Feb. 2014, Art. no. 5201907.

[12] J. Wang *et al.*, "Design of a superconducting synchronous generator with LTS field windings for 12 MW offshore direct-drive wind turbines," *IEEE Trans. Ind. Electron.*, vol. 63, no. 3, pp. 1618–1628, Mar. 2016.

[13] J. Sun, S. Sanz, and H. Neumann, "Conceptual design and thermal analysis of a modular cryostat for one single coil of a 10 MW offshore superconducting wind turbine," *IOP Conf. Ser. Mater. Sci. Eng.*, vol. 101, no. 1, 2015, Art. no. 012088.

[14] D. Liu, H. Polinder, A. B. Abrahamsen, and J. A. Ferreira, "Potential of partially superconducting generators for large direct-drive wind turbines," *IEEE Trans. Appl. Supercond.*, vol. 27, no. 5, Aug. 2017, Art. no. 5203711.

[15] Y. Wang, J. Sun, Z. Zou, Z. Wang, and K. T. Chau, "Design and analysis of a HTS flux-switching machine for wind energy conversion," *IEEE Trans. Appl. Supercond.*, vol. 23, no. 3, Jun. 2013, Art. no. 5000904.

[16] Y. Wang, Q. Feng, X. Lin, and W. Ma, "Design, analysis, and experimental test of a segmented-rotor high-temperature superconducting flux-switching generator with stationary seal," *IEEE Trans. Ind. Electron.*, vol. 65, no. 11, pp. 9047–9055, Nov. 2018.

[17] Y. Wang, M. Chen, T. W. Ching, and K. T. Chau, "Design and analysis of a new HTS axial-field flux-switching machine," *IEEE Trans. Appl. Supercond.*, vol. 25, no. 3, pp. 1–5, Jun. 2015.

[18] X. Li, S. Liu, and Y. Wang, "Design and analysis of a stator HTS field-modulated machine for direct-drive applications," *IEEE Trans. Appl. Supercond.*, vol. 27, no. 4, pp. 1–5, Jun. 2017.

[19] X. Li, S. Liu, and Y. Wang, "Design and analysis of a new HTS dual-rotor flux-switching machine," *IEEE Trans. Appl. Supercond.*, vol. 27, no. 4, pp. 1–5, Jun. 2017.

[20] Y. Wang, G. Yang, X. Zhu, X. Lin, and W. Ma, "Electromagnetic characteristics analysis of a high-temperature superconducting field-modulation double-stator machine with stationary seal," *Energies*, vol. 11, no. 5, p. 1269, May 2018.

[21] X. Li, S. Yu, and Y. Wang, "A novel HTS claw-pole Vernier machine using single excitation unit with stationary seal," *IEEE Trans. Appl. Supercond.*, vol. 29, no. 5, pp. 1–5, Aug. 2019.

[22] Y. Du, K. T. Chau, M. Cheng, Y. Wang, and J. Li, "A linear doubly-salient HTS machine for wave energy conversion," *IEEE Trans. Appl. Supercond.*, vol. 21, no. 3, pp. 1109–1113, Jun. 2011.

[23] Y. Du, K. T. Chau, M. Chengm, Y. Fan, W. Zhao, and F. Li, "A linear stator permanent magnet Vernier HTS machine for wave energy conversion," *IEEE Trans. Appl. Supercond.*, vol. 22, no. 3, Jun. 2012, Art. no. 5202505.

[24] F. Xiao, Y. Du, Y. Wang, M. Chen, T. W. Ching, and X. Liu, "Modeling and analysis of a linear stator permanent-magnet Vernier HTS machine," *IEEE Trans. Appl. Supercond.*, vol. 25, no. 3, Jun. 2015, Art. no. 5202104.

[25] X. Li, X. Wang, and Y. Wang, "Design and analysis of a new HTS linear flux-controllable doubly salient machine," *IEEE Trans. Appl. Supercond.*, vol. 29, no. 5, Aug. 2019, Art. no. 5201605.

[26] W. Ma, X. Wang, Y. Wang, and X. Li, "A HTS-excitation modular flux-switching linear machine with static seals," *IEEE Access*, vol. 7, no. 1, pp. 32009–32018, Dec. 2019.

[27] M. Cheng, P. Han, and W. Hua, "General airgap field modulation theory for electrical machines," *IEEE Trans. Ind. Electron.*, vol. 64, no. 8, pp. 6063–6074, Aug. 2017.

[28] Z. Q. Zhu, Z. Z. Wu, D. J. Evans, and W. Q. Chu, "Novel electrical machines having separate PM excitation stator," *IEEE Trans. Magn.*, vol. 51, no. 4, Apr. 2015, Art. no. 8104109.

[29] H. Yamasaki, N. Natori, and M. Furuse, "Evaluation of heat inleak in a model superconducting coil module for a wind turbine generator with iron cores," *IEEE Trans. Appl. Supercond.*, vol. 25, no. 3, Jun. 2015, Art. no. 5201405.

[30] E. Stehouwer and G. J. Zinderen, "Conceptual nacelle designs of 10-20 MW wind turbines," Project FP7-ENERGY-2012-1-2STAGE, INNWIND.EU, Deliverable D3.41, DTU Wind, Oct. 2016.

[31] X. Zhu, Z. Xiang, L. Quan, W. Wu, and Y. Du, "Multimode optimization design methodology for a flux-controllable stator permanent magnet memory motor considering driving cycles," *IEEE Trans. Ind. Electron.*, vol. 65, no. 7, pp. 5353–5366, Jul. 2018.

[32] Z. Z. Wu and Z. Q. Zhu, "Analysis of air-gap field modulation and magnetic gearing effects in switched flux permanent magnet machines," *IEEE Trans. Magn.*, vol. 51, no. 5, May 2015, Art. no. 8105012.

[33] X. Sun, Y. Shen, S. Wang, G. Lei, Z. Yang, and S. Han, "Core losses analysis of a novel 16/10 segmented rotor switched reluctance BSG motor for HEVs using nonlinear lumped parameter equivalent circuit model," *IEEE/ASME Trans. Mechatronics*, vol. 23, no. 2, pp. 747–757, Apr. 2018.

[34] X. Sun *et al.*, "Perform ance analysis of suspension force and torque in an IBPMSM with V-shaped PMS for flywheel batteries," *IEEE Trans. Magn.*, vol. 54, no. 11, Nov. 2018, Art. no. 8105504.

[35] X. Sun *et al.*, "Performance improvement of torque and suspension force for a novel five-phase BFSPM machine for flywheel energy storage systems," *IEEE Trans. Appl. Supercond.*, vol. 29, no. 2, Mar. 2019, Art. no. 0601505.

[36] H. Polinder, "Final assessment of superconducting (SC) and pseudo direct drive (PDD) generator performance indicators (PI's)," Project FP7-ENERGY-2012-1-2STAGE, INNWIND.EU, Deliverable D3.44, DTU Wind, Oct. 2017.

[37] A. F. Diaz *et al.*, "Study of improvements in the critical components of the 10 MW SC generator," Project SUPRAPOWER, Deliverable D5.1, May 2017.

XINKAI ZHU (S'15) received the B.S. degree in electrical engineering from the Shenyang University of Technology, Shenyang, China, in 2015. He is currently pursuing the Ph.D. degree in electrical engineering with the School of Electrical Engineering, Southeast University, Nanjing, China.

From 2019 to 2020, he will be a guest Ph.D. Student funded by the China Scholarship Council with the Center for Electric Power and Energy, Technical University of Denmark, Copenhagen, Denmark, where he focuses on AC loss calculation and quench analysis of superconducting coil applied in wind generator. His current research interests include design and analysis of superconducting electrical machine, and wind power generation systems.

MING CHENG (M'01–SM'02–F'15) received the B.Sc. and M.Sc. degrees from the Department of Electrical Engineering, Southeast University, Nanjing, China, in 1982 and 1987, respectively, and the Ph.D. degree from the Department of Electrical and Electronic Engineering, The University of Hong Kong, Hong Kong, in 2001, all in electrical engineering.

Since 1987, he has been with Southeast University, where he is currently a Chair Professor with the School of Electrical Engineering, and the Director of the Research Center for Wind Power Generation. He was a Visiting Professor with the Wisconsin Electric Machine and Power Electronics Consortium, University of Wisconsin-Madison, Madison, WI, USA, in 2011, and a Visiting Professor with Aston University, U.K., from 2016 to 2019. His teaching and research interests include electrical machines, motor drives for EV, and renewable energy generation. He has authored or coauthored over 400 technical papers and four books, and is the holder of 120 patents in these areas.

Prof. Cheng is a Fellow of the Institution of Engineering and Technology. He has served as the Chair and an Organizing Committee Member for many international conferences. He is a Distinguished Lecturer of the IEEE Industry Application Society, in 2015–2016.